AUT Journal of Electrical Engineering
10.22060/EEJ.2026.25020.5820

Hybrid RST-Direct Thrust Force Control for Enhanced Performance of Linear Induction Motor

Laid Khettache*, Abdeslam Benmakhlouf, Mohamed Redha Rezoug, Djalal Djarah

Department of Electrical Engineering, Kasdi Merbah Ouargla University, Algeria.
*Corresponding author e-mail: khettache.laid@univ-ouargla.dz

Abstract:

This paper presents a novel control strategy that combines RST-based speed control with Direct Thrust Force Control to improve the operational performance of linear induction motors. This approach specifically targets the optimization of thrust force, magnetic flux, and current control. While traditional PID controllers are commonly used in direct torque control applications for rotary motors, their effectiveness in linear induction motors is limited by sensitivity to parameters and nonlinear effects caused by end-effect phenomena. These limitations frequently result in excessive overshoot, slower rise and settling times, as well as reduced control accuracy and system stability. In response, this study proposes the RST- Direct Thrust Force Control method, which is designed to achieve robust speed regulation and precise control over thrust force and flux under various operating conditions. The performance and accuracy of the proposed approach are evaluated and validated through simulations conducted in the MATLAB/Simulink environment. Moreover, comparative simulation analyses demonstrate that the RST-Direct Thrust Force Control technique significantly reduces overshoot, shortens rise and settling times, and confirming its superiority in maintaining control precision, including excellent reference tracking and disturbance rejection. The findings highlight the RST regulator combined with the Direct Thrust Force Control technique as a robust solution for overcoming the inherent limitations of conventional direct torque control in linear induction motor applications. This integrated control presents a promising approach to optimizing linear induction motor performance and aligns with industry demands for precision and reliability in dynamic environments.

AI Declaration: During the preparation of this manuscript, the authors used ChatGPT (OpenAI) solely to improve the English language, grammar, and readability of the text. The AI tool was not used to generate the research methodology, simulations, data analysis, results, or conclusions. The authors take full responsibility for the scientific content of this manuscript.

Keywords: Thrust Optimization; RST controller; linear motors; speed control; end-effect

1. Introduction

Linear induction motors (LIMs) have become increasingly important in applications requiring precise and efficient linear motion, such as transportation systems, robotics, and material handling, due to their ability to produce linear motion without requiring mechanical conversion mechanisms [1]. Unlike rotary induction motors, these advantages, combined with their robustness and low maintenance requirements, make LIMs highly suitable for dynamic and high-precision environments [2]. However, the complex dynamics and parameter variations of LIMs such as end-effect, variable coupling and nonlinear characteristics present significant challenges for effective control strategies. To address these challenges, advanced control methods that ensure precise speed, robust thrust force control, and system stability are required. Among these methods, Direct Torque Control (DTC) is a high-performance control strategy widely used in electric motors for its simplicity, fast dynamic response, and effective control of torque and flux without relying on complex coordinate transformations [3]. In the case of LIMs, the DTC technique is adapted as Direct Thrust Force Control (DTFC), which is similar to DTC but is specifically used to control the thrust force and flux. DTFC offers a rapid response to changes in thrust force demands and robust control of the electromagnetic characteristics, making it a powerful choice for the inner force control loop. In the literature [4,5], DTC based PI regulator has certain limitations. It often causes overshoot during startup, load and unload condition, which reduces overall performance. Additionally, the PI controller is sensitive to changes in motor parameters, which can lead to decreased accuracy and reliability in control. In light of this limitation and the drawbacks associated with variations in motor parameters, an RST polynomial controller has been developed. This controller, based on polynomial control theory employed three polynomials R, S, and T to shape the closed-loop response as desired [6,7]. This structure offers greater flexibility, enabling improved control of transient responses and enhanced robustness against variations in motor parameters. The main novelty of this research work lies in the development and application of an RST-based speed regulation layer combined with a DTFC inner loop for LIMs, specifically addressing the end-effect problem and improving overall drive performance. This integrated RST–DTFC structure has not been widely explored in existing literature for LIM speed control. Through simulation studies, the proposed method demonstrates significant improvements in control accuracy, dynamic response, and robustness, making it suitable for high-performance industrial and transportation applications. This paper is structured as follows: Section 2 outlines the dynamic model of the LIM in the α-β coordinate system, which is essential for understanding the motor's behavior. While section 3 explains the theoretical principles of the direct thrust force control (DTFC) strategy for regulating flux and thrust force of LIM. Section 4 discusses the structure and implementation of the polynomial RST regulator used to ensure stability and achieve the desired dynamic response of rotor speed. Section 5. Evaluates the performance and robustness of the proposed RST-DTFC method through MATLAB/SIMULINK with comparative analysis to confirm the technique's efficiency. Finally, Section 6 summarizes the key findings and emphasizing the practical implications of the approach in improving LIM performance, and concludes the paper.

2. Modeling of a Linear Induction Motor

The linear induction motor (LIM) operates on the same fundamental principle as a conventional rotary induction motor, wherein the stator generates a magnetic field that induces currents in the secondary component (commonly referred to as the rotor) [8]. However, in contrast to rotary induction motors, the LIM is specifically designed to produce linear motion rather than rotational motion. Besides, the modeling of a linear induction motor (LIM) is crucial for understanding its operational behavior, evaluating its performance, and developing efficient control systems. This process is based on mathematical formulations as well as on considering the end-effect phenomena. The dynamic model of the LIM, as described by Gieras et al. [9], and Faiz et al. [10], is developed in the d-q reference frame of the equivalent electrical circuit.

To simplify the analysis of the LIM and reduce the complexity of the dynamic model, the linkage flux equations in the α-β reference frame are given by:

$$\begin{cases} \phi_{\alpha s} = L_{ls} i_{\alpha s} + L_m \left(1 - f\left(Q\right)\right)\left(i_{\alpha s} + i_{\alpha r}\right) \\ \phi_{\beta s} = L_{ls} i_{\beta s} + L_m \left(i_{\beta s} + i_{\beta r}\right) \\ \phi_{\alpha r} = L_{lr} i_{\alpha r} + L_m \left(1 - f\left(Q\right)\right)\left(i_{\alpha r} + i_{\alpha s}\right) \\ \phi_{\beta r} = L_{lr} i_{\beta r} + L_m \left(i_{\beta r} + i_{\beta s}\right) \end{cases} \tag{1}$$

One of the major challenges in the modeling of linear induction motors (LIMs) is the consideration of end effects. These phenomena, caused by the physical termination of the linear windings, result in flux leakage and distortions in the magnetic field.

In [11], Q is a crucial parameter for describing the end-effects phenomenon.

$$Q = \frac{D.R_r}{\left(L_m + L_{lr}\right).v} \tag{2}$$

When considering the eddy current losses, a resistance that emerges in the transverse branch is defined as:

$$\hat{R}_r = R_r f\left(Q\right) \tag{3}$$

Where: $f\left(Q\right)$ is a correction factor defined as:

$$f\left(Q\right) = \frac{1 - e^{-Q}}{Q} \tag{4}$$

The magnetizing inductance which depends on the end-effects (Q) is given by:

$$\hat{L}_m = L_m\left[1 - f\left(Q\right)\right] \tag{5}$$

The conversion of the linear induction motor's (LIM) angular speed (ωr) to its linear velocity (v) is represented by the following equation:

$$v = \frac{\tau_p}{\pi}\omega_r \tag{6}$$

where τ_p denotes the pole pitch of the LIM.

The electromagnetic force (*Fe*) generated by the linear induction motor (LIM) can be expressed as:

$$F_e = \frac{3\pi}{2\tau_p}\frac{p}{2}\left(\phi_{\alpha r} i_{\beta r} - \phi_{\beta r} i_{\alpha r}\right) \tag{7}$$

The motion equation of the Linear Induction Motor (LIM) is given by:

$$M\frac{d}{dt}v + B.v = F_e - F_L \tag{8}$$

3. Direct Thrust Force Control

The adaptation of Direct Thrust Force Control (DTFC) for linear induction motors (LIM) is based on principles analogous to those of Direct Torque Control (DTC) used in rotary motors. However, DTFC specifically addresses the inherent characteristics of linear motion by focusing on linear force instead of torque. On the other hand, DTFC is founded on the principle of stator flux orientation [12]. This methodology facilitates the determination of control variables, such as stator flux and electromagnetic force. It uses only stator current and voltage measurements without requiring mechanical sensors. (see Fig.1).

The control sequence applied to the voltage inverter switches is determined directly without requiring complex intermediate steps. It relies on hysteresis controllers to maintain the system variables within predefined limits by simultaneously regulating the amplitude of the stator flux and the electromagnetic force,[13].

The primary flux estimation $\hat{\phi}_s$ is carried out from the stator voltage equations, expressed in a fixed frame (α-β). This estimation is obtained by integrating the components of the stator voltage:

$$\begin{cases} \phi_{\alpha s} = \int \left(V_{\alpha s} - R_s i_{\alpha s} - R_r f\left(Q\right)\left(i_{\alpha s} + i_{\alpha r}\right)\right).dt \\ \phi_{\beta s} = \int \left(V_{\beta s} - R_s i_{\beta s}\right).dt \end{cases} \tag{9}$$

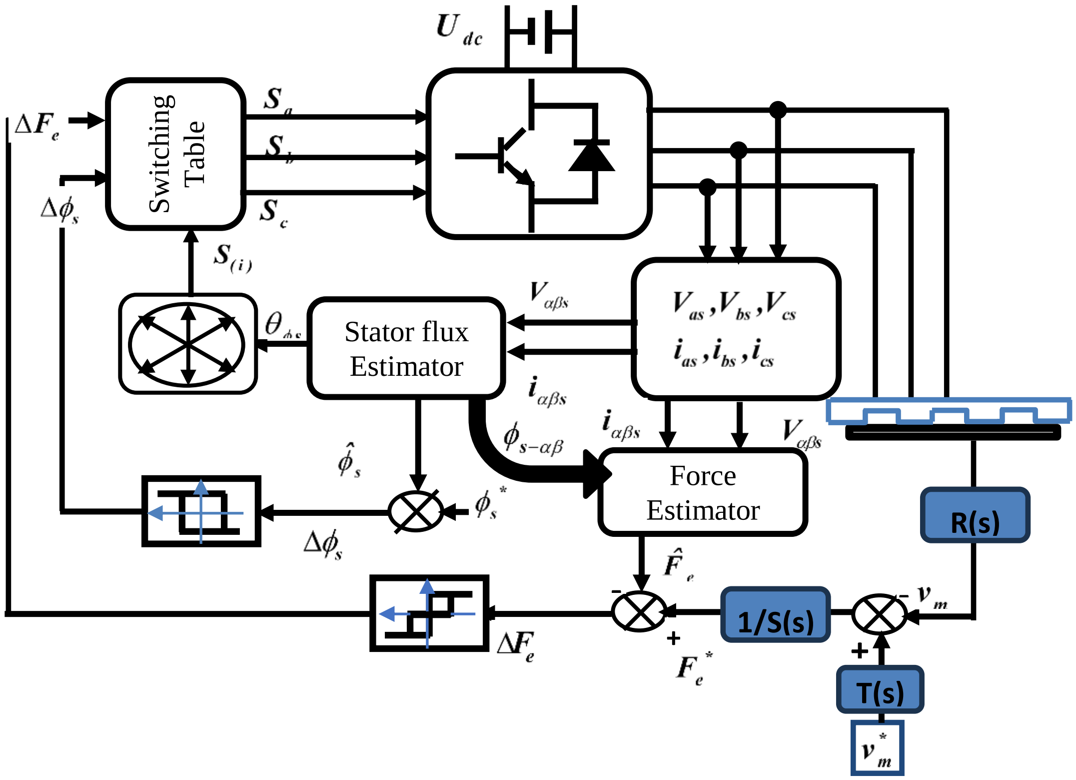

Fig. 1. Block Diagram of DTFC control and RST Regulator For LIM

The magnitude and angle of the stator flux, which are fundamental for flux orientation and direct control, are defined as follows:

$$\left|\hat{\phi}_s\right| = \sqrt{\phi_{\alpha s}^2 + \phi_{\beta s}^2} \tag{10}$$

$$\theta_{\phi s} = Arctg\,\frac{\phi_{\beta s}}{\phi_{\alpha s}} \tag{11}$$

where $\phi_{\alpha s}$ and $\phi_{\beta s}$ represent the components of the stator flux in the (α-β) reference frame.

The electromagnetic thrust force is determined by the vector product of the stator's primary current and magnetic flux. In the stationary reference frame (α-β), the estimated thrust force is calculated as follows:

$$\hat{F}_e = \frac{3\pi}{2\tau_p}\frac{p}{2}\left(\phi_{\alpha s} i_{\beta s} - \phi_{\beta s} i_{\alpha s}\right) \tag{12}$$

The flux error $\Delta\phi_s$, defined as the difference between the reference flux ϕ_s^* and the estimated flux $\hat{\phi}_s$, is processed using a two-level hysteresis regulator. This regulator can assume two states, 0 or 1, to maintain the flux within predefined limits.

Similarly, the thrust force error ΔF_e, calculated as the difference between the reference thrust force F_e^* and the estimated thrust force $\hat{F}_e$, is processed using a three-level hysteresis regulator. This regulator can take values of -1, 0, or 1, providing precise and rapid control.

In the complex plane, voltage vectors are arranged to form a hexagon. Each active vector (V1 to V6) corresponds to a specific direction in the plane, while the zero vectors (V0 and V7) are positioned at the center of the hexagon [14].

Subsequently, a switching table (Table 1) establishes a correlation between the states of the flux error ($\Delta\phi_s$) and the thrust force error (ΔF_e), as well as the corresponding voltage vector. This association is based on the angular position of the stator flux within predefined sectors. The logic table ensures optimal inverter control, enabling precise and rapid regulation of both flux and thrust force. It minimizes oscillations and enhances the overall dynamic performance of the motor.

Table 1. Switching Table of Voltage Vectors Selection

$\Delta\phi_s$	ΔF_e	Sector					
		I	II	III	IV	V	VI
1	1	V2	V3	V4	V5	V6	V1
	0	V7	V0	V7	V0	V7	V0
	-1	V6	V1	V2	V3	V4	V5
0	1	V3	V4	V5	V6	V1	V2
	0	V0	V7	V0	V7	V0	V7
	-1	V5	V6	V1	V2	V3	V4

4. RST Controller

The RST controller gets its name from the three polynomials *R(s)*, *S(s)*, and *T(s)*. It is commonly used to improve tracking performance, disturbance rejection, and robustness in various applications, such as motor control and power electronics [15].

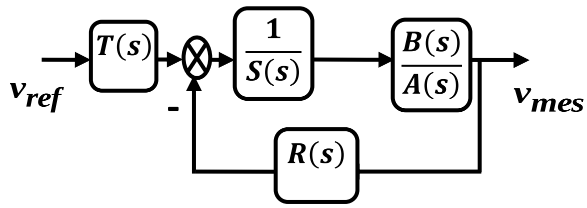

Fig.2. RST closed loop configuration

Fig.2. Depicts the RST regulator architecture within a closed-loop control framework. The regulator design is formulated using a polynomial synthesis approach, where the individual components are defined as follows:

R(s): Designed to ensure the stabilization of poles within the linear induction motor (LIM).

S(s): is chosen to provide disturbance rejection, especially against load variations.

T(s): Calibrated to achieve precise speed tracking, ensuring the LIM accurately follows the specified speed reference.

The Diophantine equation plays a crucial role in the design of the RST controller, which sets a relationship between the desired closed-loop poles and the polynomials. It can be expressed as:

$$A(s)S(s) + B(s)R(s) = P(s) \tag{13}$$

where:

A(s) and *B(s)* represent the transfer function polynomials of the plant.

P(s) denotes the desired characteristic polynomial, which corresponds to the placement of closed-loop poles.

In the context of the linear induction motor (LIM) speed, the denominator *A(s)* and the numerator *B(s)* of the transfer function for rotor speed are defined as follows:

$$\begin{cases} A(s) = M.s + f_r \\ B(s) = 1 \end{cases} \tag{14}$$

When: $deg(R) = deg(A) = 1$ and $deg(S) = deg(A) + 1$

The polynomials *R(s), S(s)* it can expressed by:

$$\begin{cases} R(s) = r_1 s + r_0 \\ S(s) = s_2 s^2 + s_1 s \\ T(s) = R(0) \end{cases} \tag{15}$$

The determination of the coefficients for *R(s)* and *S(s)*, the desired closed-loop *P(s)* characteristic polynomial is defined by:

$$P(s) = p_0 + p_1 s + p_2 s^2 + p_3 s^3 \tag{16}$$

Based on the Diophantine Eq. (13), and by substituting the polynomial expressions given in Eq. (15), the closed-loop characteristic equation can be written as:

$$(M\ s + f_r).(s_2 s^2 + s_1\ s) + 1.(r_1\ s + r_0) = P(s) \tag{17}$$

After polynomial expansion, the following expression is obtained:

$$M\ s_2\ .s^3 + (Ms_1 + f_r s_2).s^2 + (f_r s_1 + r_1).s + r_0 = P(s) \tag{18}$$

By identifying the coefficients of Eq. (18) with those of the desired characteristic polynomial in Eq. (16), a system of algebraic equations is obtained. The coefficients of the *R(s)* and *S(s)* polynomials can then be computed using the Sylvester matrix method, as follows:

$$\begin{bmatrix} \mathbf{p}_0 \\ \mathbf{p}_1 \\ \mathbf{p}_2 \\ \mathbf{p}_3 \end{bmatrix} = \begin{bmatrix} \mathbf{M} & 0 & 0 & 0 \\ \mathbf{f_r} & \mathbf{M} & 0 & 0 \\ 0 & \mathbf{f_r} & 1 & 0 \\ 0 & 0 & 0 & 1 \end{bmatrix} * \begin{bmatrix} \mathbf{s}_2 \\ \mathbf{s}_1 \\ \mathbf{r}_1 \\ \mathbf{r}_0 \end{bmatrix} \tag{19}$$

Solving this system yields the controller coefficients:

$$\begin{cases} r_0 = p_0 \\ r_1 = p_1 - f_r.s_1 \\ s_1 = \dfrac{p_2 - f_r.s_2}{M} \\ s_2 = \dfrac{p_3}{M} \end{cases} \tag{20}$$

5. PI Controller

In this section, the initial determination of the PI controller parameters is carried out by defining specific performance criteria, such as the damping ratio (ζ) and natural frequency (ωn), this approach provides a mathematically rigorous starting point that ensures the system operates within a stable region. The control loop of speed is modeled according to its specific physical time constants, and the gains are calculated by mapping the closed-loop poles to a desired characteristic equation:

$$s^2 + 2\zeta\omega_n s + \omega_n{}^2 = 0 \tag{21}$$

For the mechanical dynamics of the linear induction motor, the speed loop can be represented by the following characteristic equation:

$$s^2 + \frac{f_r + K_p}{M} s + \frac{K_i}{M} = 0 \tag{22}$$

With the selected damping ratio ζ=0.7, the natural frequency ωn can be estimated using the settling time Ts criterion according to the standard second-order system relationship:

$$\omega_n = \frac{4}{\zeta T_s} \tag{23}$$

The PI controller gains for speed regulation are then determined as follows:

$$\begin{cases} K_{p\omega} = 2\zeta\omega_{n\omega}M - f_r \\ K_{i\omega} = M\,\omega_{n\omega}^{\;2} \end{cases} \tag{24}$$

6. Results and discussions

In this section, computer simulations were carried out to evaluate the performance and effectiveness of the proposed method. Two tests tracking and robustness were performed using the MATLAB/Simulink environment. The parameters of the Linear Induction Motor (LIM) used in the simulation, along with the gains of the RST and PI regulators applied to speed control are listed in Tables 4 and 5 (Appendix), respectively. Furthermore, the performance of the RST and PI regulators in the Direct Thrust Force Control (DTFC) framework was evaluated under specific dynamic conditions. The reference speed was increased from 2.8 m/s to 4 m/s at t=0.5 sec, while the thrust force was changed from 10 N to 20 N at t=0.3 sec. These tests were designed to validate the robustness and accuracy of the proposed control strategies under varying operational conditions.

6.1. Test tracking performance

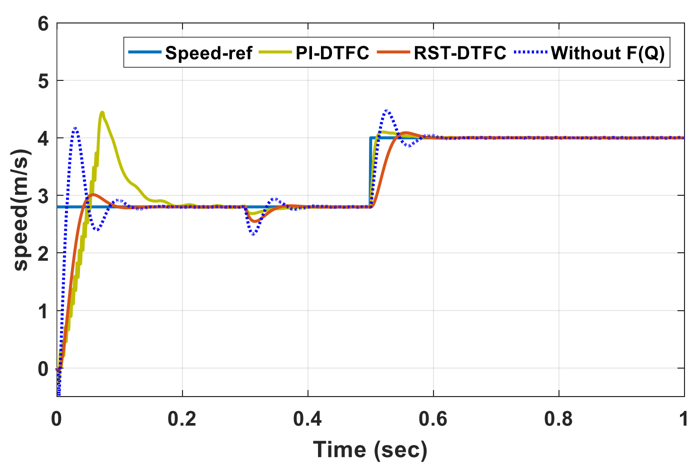

Fig.3. Response of the linear rotor speed variation with and without end-effect *f(Q)*

Fig.3. Shows that the measured speeds obtained by the two controllers closely track their respective speed references (blue line) and quickly reject disturbances caused by a load force at time t = 0.5 sec, with minimal steady-state error.

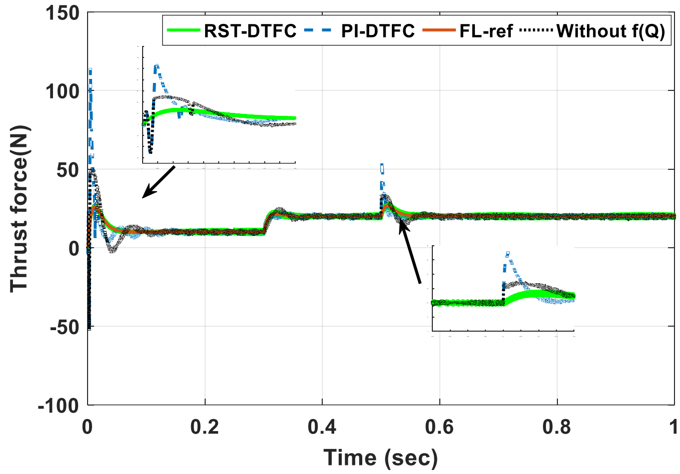

Fig.4. Thrust force response under thrust load FL variations.

Similarly, in Fig.4. Both regulators show satisfactory thrust force tracking, with a notable reduction in ripple. However, the PI regulator exhibits significantly higher values at startup, while the force ripple is substantially minimized when employing RST controller techniques.

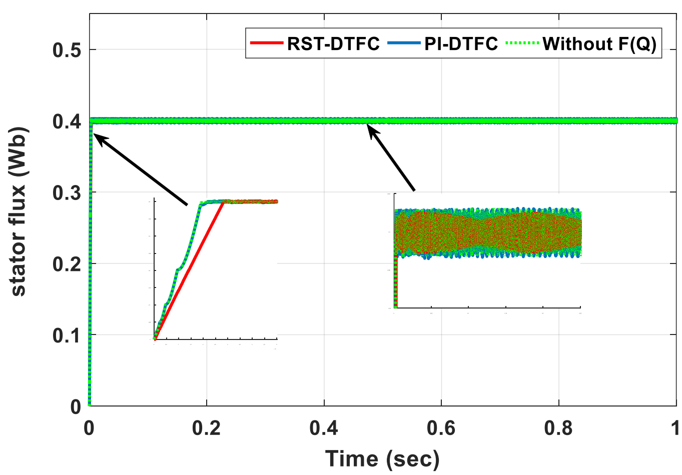

Fig. 5 –Flux stator response

Moreover, Fig.5. Illustrates an effective decoupling control between force and flux, wherein the stator flux is maintained at the corresponding reference flux of $\phi_s^* = 0.4$ Wb.

Furthermore, the comparative analysis conducted under both conditions (with and without the incorporation of the end-effect compensation *f(Q))* provides compelling evidence of the performance superiority of the proposed RST-DTFC over the conventional PI-DTFC. It is clearly observed that the RST-based control achieves markedly enhanced closed-loop stability and significantly higher reference-tracking precision. This improvement is primarily attributed to the inherent capacity of the RST polynomial controller to actively attenuate the nonlinear disturbances caused by the end-effect phenomenon, which constitutes a critical source of performance degradation in linear induction motor (LIM) drives. In contrast, the conventional PI-DTFC demonstrates a notable degradation in tracking accuracy when subjected to identical operating conditions. Consequently, the proposed RST-DTFC strategy not only mitigates these adverse effects through its structured polynomial design but also ensures consistent dynamic performance across a broad range of operating regimes, thereby confirming its practical suitability for high-performance linear drive applications.

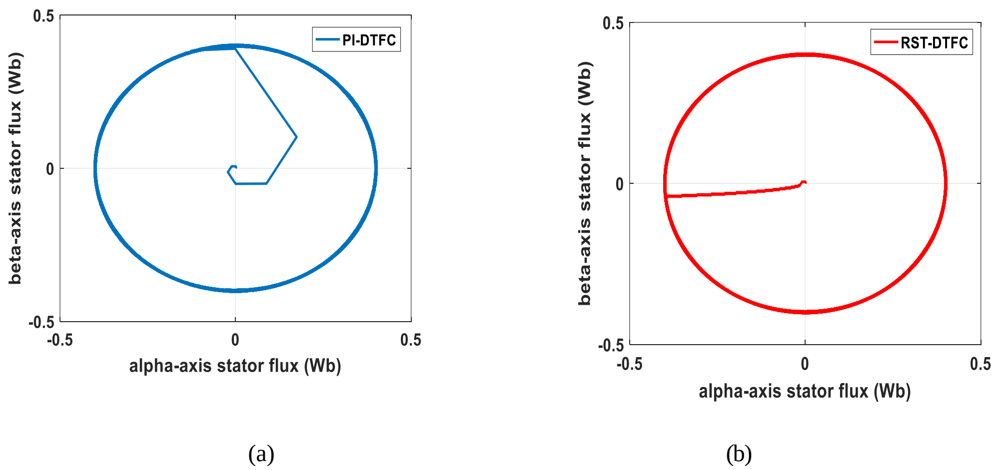

Fig.6. Circular trajectory of stator field (alpha and beta): (a) conventional DTFC; (b) proposed structure DTFC-RST.

Fig.6. Illustrates the circular trajectory of the stator flux. It demonstrates that the proposed RST-DTFC method provides clear advantages over the conventional DTFC by significantly reducing flux ripple and achieving more accurate flux reference tracking.

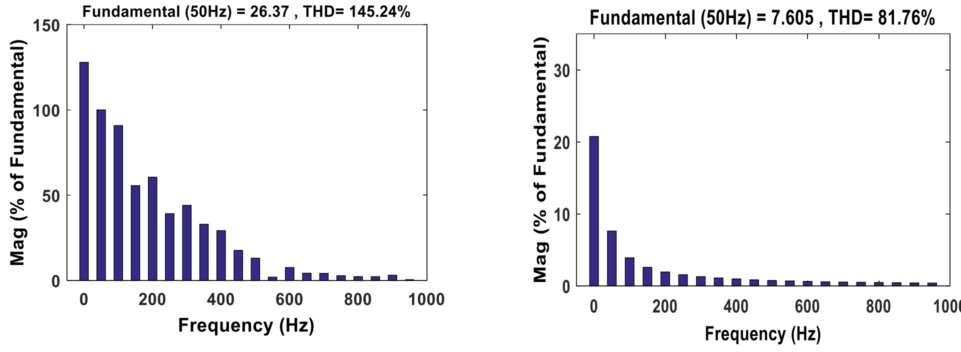

(a) (b)

Fig.7. The harmonic spectrum for both DTFC techniques: a). based-PI; b) based- RST.

The FFT analysis in Fig.7 reveals a notable reduction in total harmonic distortion (*THD*). The proposed DTFC technique with the RST regulator achieves a *THD* of 81.76% (Fig. 7.b), significantly lower than the 145.24% observed in the conventional DTFC method (Fig. 7.b). These results highlight the superior harmonic performance of the proposed approach. It is evident that the proposed RST controller outperforms the classical PI controller in terms of overshoot, rise time, settling time, and rejection of external forces as seen in table 2.

6.2. Robustness test

To evaluate the robustness of the proposed controllers, both regulators were tested under a 50% increase in stator resistance (*Rs*) and a 100% increase in motor mass (*M*).

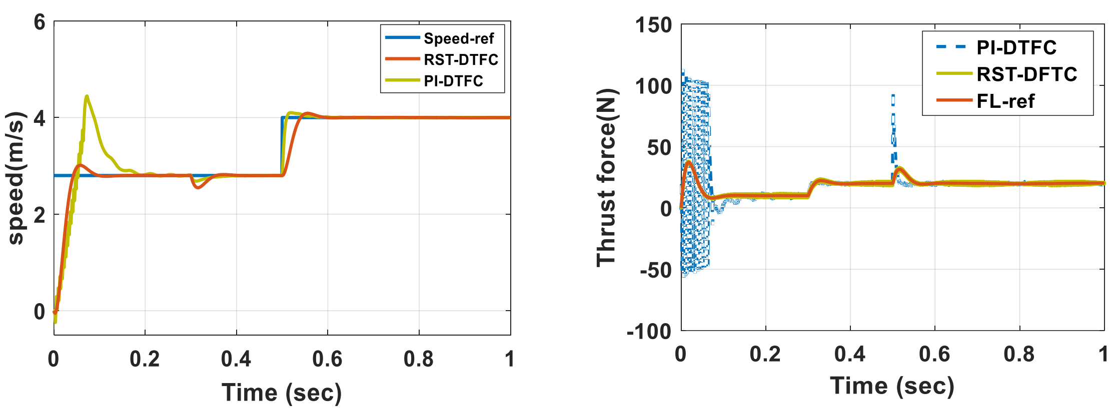

(a) (b)

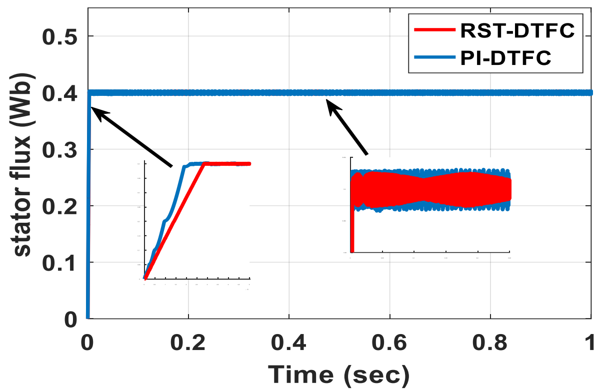

(c)

Fig.8. Comparative Responses under +50% Increase in Rs and +100% in M. (a) Rotor speed, (b) Thrust force, (c) Stator Flux

From Fig.8, the PI regulator exhibited high overshoot, reaching 58.77%, along with prolonged settling times, indicating instability and oscillatory behavior during transitions. This was particularly evident in thrust force tracking, which demonstrated poor robustness under dynamic conditions. In contrast, the RST regulator maintained stable control, with minimal overshoot and faster settling times, showcasing its robustness to parameter variations and load disturbances. The following table presents comparative performance metrics between the proposed RST-DTFC approach and the conventional PI-DTFC technique.

Table 2. Comparative Analysis of Rotor Speed Performance

Method of control		Rs (Ω) and M (kg)	Rs (Ω) +50% and M (kg)+100%
PI-DTFC	Overshoot-	14.54%	58.77%
	Rise time-	0.0087	0.049
	Peak	3.2108	4.4461
	Settling time-	0.0842	0.177
	Steady-State Error	0.0114	0.0159
	RMS thrust ripple	20.27	20.46
RST-DTFC	Overshoot %	0.1092%	7.6645%
	Rise time-	0.0275	0.0259
	Peak	2.8045	3.0118
	Settling time-	0.0487	0.0845
	Steady-State Error	0.0057	0.0096
	RMS thrust ripple	19.34	20.24

In light of these significant findings, a comparative analysis with previously reported DTFC-based Linear Induction Motor (LIM) control methods available in the literature is presented in Table 3. The comparison focuses on several important aspects, including end-effect consideration, robustness validation, thrust ripple reduction capability, and the main limitations of existing approaches.

Table 3. Comparative Analysis Between the Proposed RST-DTFC Method and Existing DTFC-Based LIM Control Strategies

Ref.	Method	End-Effect Considered	Robustness Analysis	Ripple Reduction	Main Limitation
[17]	Conventional DTFC	Yes	Limited	Moderate	High ripple
[18]	DTFC	Yes	No	Moderate	Sensitive to parameters
[19]	Sensorless DTFC	Partial	Limited	Moderate	Complex estimator
Our wok	RST-DTFC	Yes	+50% Rs and +100% M	High	Higher computation

As can be observed, most previously published DTFC methods suffer from limitations related to parameter sensitivity, insufficient robustness analysis, or weak disturbance rejection capability. In contrast, the proposed RST-DTFC approach explicitly incorporates longitudinal end-effect compensation and demonstrates enhanced robustness under severe operating conditions, including +50% stator resistance variation and +100% mass variation. Furthermore, the proposed method achieves improved thrust ripple mitigation and superior dynamic performance compared with conventional DTFC structures.

7. Conclusion

This paper presents a novel approach to controlling a linear induction motor (LIM) through a combination of the direct thrust force control (DTFC) technique and a polynomial RST regulator. In contrast to the conventional direct torque control (DTC) used for rotary induction motors (RIMs), the proposed method improves the flux and thrust equations by accounting for end effects and incorporates these improvements into the flux and thrust force estimator. The DTFC approach allows for the independent regulation of the force and magnetizing flux components produced by the motor. To improve the control process, we propose an effective strategy based on a polynomial RST regulator. This approach (DFTC-RST) is specifically designed to mitigate the impacts of parameter variations and external disturbances. The results obtained through Matlab Simulink confirm the superior performance of the RST-DTFC regulator in both tracking and robustness tests. Its precise control, stability, and adaptability make it the preferred choice for linear induction motor applications, especially in dynamic and uncertain environments. Furthermore, this research identifies potential areas for future investigation, such as the integration of artificial intelligence techniques for adaptive and intelligent control of linear induction motors. In addition, future work will include experimental implementation and PSCAD/EMTDC validation to further verify the effectiveness, robustness, and practical applicability of the proposed RST-DTFC controller under real-time electromagnetic transient operating conditions.

Appendices

Table 4. Main Parameters of Linear Induction Motor

Parameters	Values
R_s	1.25 Ω
R_r	2.7 Ω
L_{ls}	40.1 mH
L_{lr}	33.1 mH
L_m	32.6 mH
τ_p	0.0641 m
D	0.286 m
M	8 kg
p	4

Table 5. Regulator values

RST	PI
$r_0 = 9292.5$	*Kp=35.64*
$r_1 = 5256$	*Ki=106.3*
$s_1 = 375$	/
$s_1 = 0.12$	/

8. Nomenclature

$V_{\alpha s}, V_{\beta s}$: Primary (stator) voltages in the $\alpha-\beta$ axes (Volts)

$i_{\alpha s}, i_{\beta s}, i_{\alpha r}, i_{\beta r}$: $\alpha-\beta$ axes primary (stator) and Linor (rotor) currents (A)

$\phi_{\alpha s}, \phi_{\beta s}, \phi_{\alpha r}, \phi_{\beta r}$: $\alpha-\beta$ axes stator and rotor flux linkages (Wb)

L_s, L_r Stator and rotor self-inductances (H)

R_s, R_r: Stator and rotor resistances (Ω)

Q: Factor associated with the length of rotor

F_e: Electromagnetic force (thrust force)

τ_p: Pole pitch (m)

D: Length of the linor (m)

p: No of poles

v: Velocity (m/s)

ω_r: Rotor angular velocity (rad/sec)

$\sigma, \sigma^{'}$: Leakage coefficients with and without end-effect

fr : Viscous Friction Coefficient

9. References

[1] M. F. Elmorshedy, D. Almakhles, and S. M. Allam, "Improved performance of linear induction motors based on optimal duty cycle finite-set model predictive thrust control," Heliyon, 2024, vol. 10, no. 13, pp. e34169.

[2] R. Palka and K. Woronowicz, "Linear induction motors in transportation systems," Energies, 2021, vol. 14, no. 9, pp. 2549.

[3] E. L. Benyoussef and S. Barkat, "Three-level direct torque control based on balancing strategy of five-phase induction machine," Revue Roumaine des Sciences Techniques–Série Électrotechnique et Énergétique, 2022, vol. 67, no. 2, pp. 93–98.

[4] S. El Daoudi, L. Lazrak, N. El Ouanjli, and M. Ait Lafkih, "Applying sliding mode technique for the nonlinear DTC-SPWM control strategy of sensorless squirrel cage asynchronous motor," International Journal of Dynamics and Control, 2021, vol. 9, no. 4, pp. 1633–1644.

[5] S. Guedida, B. Tabbache, K. Nounou, and M. Benbouzid, "Direct torque control scheme for less harmonic currents and torque ripples for dual-star induction motor," Revue Roumaine des Sciences Techniques–Série Électrotechnique et Énergétique, 2023, vol. 68, no. 4, pp. 331–338.

[6] L. Khettache and R. Abdessemed, "A new speed control approach of linear induction motor based on robust RST controller and model reference adaptive system estimator," International Journal of Engineering, 2023, vol. 36, no. 4, pp. 630–639.

[7] A. Abdelkader, A. Chaker, and T. Allaoui, "An adaptive RST fuzzy logic and an adaptive PI fuzzy logic controller of a DFIG in wind energy conversion," Przegląd Elektrotechniczny, 2021, vol. 97, no. 11, pp. 11–20.

[8] Z. Hu, J. Xu, W. Ren, and L. Liu, "Improved vector control strategy of linear induction motors for electromagnetic launch," IET Power Electronics, 2020, vol. 13, no. 19, pp. 4659–4664.

[9] J. F. Gieras, G. E. Dawson, and A. R. Eastham, "A new longitudinal end effect factor for linear induction motors," IEEE Transactions on Energy Conversion, 1987, vol. EC-2, no. 1, pp. 152–159.

[10] J. Faiz and H. Jagari, "Accurate modeling of single-sided linear induction motor considering end effect and equivalent thickness," IEEE Transactions on Magnetics, 2000, vol. 36, no. 5, pp. 3785–3790.

[11] R. Rajan, A. Lekshmi, R. Krishna, and S. Sreeja, "Mathematical modelling and analysis of linear induction motor," in Proceedings of the IEEE International Power and Renewable Energy Conference (IPRECON), Kollam, India, 2022, pp. 1–6.

[12] A. Mousaei, M. B. Bannae Sharifian, and N. Rostami, "Direct thrust force control (DTFC) of optimized linear induction motor with super twisting sliding mode controller (STSMC)," in Proceedings of the 12th Power Electronics, Drive Systems, and Technologies Conference (PEDSTC), Tabriz, Iran, 2021, pp. 1–5.

[13] B. G. Markov and D. G. Markova, "Comparison of methods for control of linear induction motors," in Proceedings of the 55th International Scientific Conference on Information, Communication and Energy Systems and Technologies (ICEST), Niš, Serbia, 2020, pp. 141–144.

[14] F. Y. Notash, S. Khateri-Abri, N. Rostami, and S. H. Hosseini, "Direct thrust control of a linear induction motor using a reduced-switch three-level converter," in Proceedings of the 11th Power Electronics, Drive Systems, and Technologies Conference (PEDSTC), Tehran, Iran, 2020, pp. 1–6.

[15] B. Nemouchi, S. E. Rezgui, A. Babqi, A. Harrison, H. Benalla, E. Ali, and S. S. Ghoneim, "Driving an asynchronous motor powered by PV-MPPT using equivalent RST controller of fractional-order PI and IP, based on generalized predictive control," IET Generation, Transmission & Distribution, 2024, vol. 18, no. 8, pp. 1576–1589.

[16] L. Khettache, D. Djalal, G. Zidani, and R. Abdessemed, "Optimization of RST controller for speed control of linear induction motor using genetic algorithm," Recent Advances in Electrical & Electronic Engineering, 2024, vol. 17, no. 3, pp. 260–268.

[17] B. Markov, "Direct force control of the electromagnetic force of linear induction motor with end effects," in Proceedings of the XXXIII International Scientific Conference Electronics (ET), Sozopol, Bulgaria, 2024, pp. 1–6.

[18] M. A. Usta, O. Akyazi, and A. S. Akpinar, "Simulation of direct thrust control for linear induction motor including end-effect," in Proceedings of the International Symposium on Innovations in Intelligent Systems and Applications, Trabzon, Turkey, 2012, pp. 1–5.

[19] M. F. Elmorshedy, W. Xu, Y. Liu, S. M. Allam, M. M. Ali, and M. Dong, "Sensorless direct thrust control of a linear induction motor based on MRAS," in Proceedings of the 12th International Symposium on Linear Drives for Industry Applications (LDIA), Neuchâtel, Switzerland, 2019, pp. 1–6.